Published June 13, 2014

Original Research

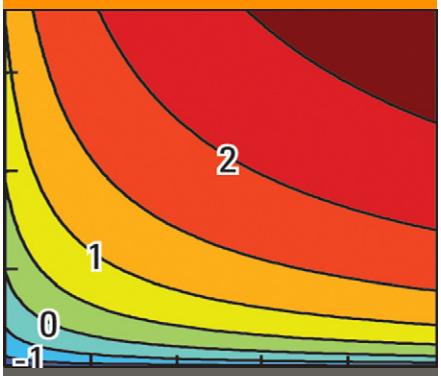

A Screening Tool for Delineating Subregions of Steady Recharge within Groundwater Models

Jesse E. Dickinson,* T.P.A. Ferré, Mark Bakker, and Becky Crompton

We have developed a screening method for simplifying groundwater models by delineating areas within the domain that can be represented using steady-state groundwater recharge. The screening method is based on an analytical solution for the damping of sinusoidal infiltration variations in homogeneous soils in the vadose zone. The damping depth is defined as the depth at which the flux variation damps to 5% of the variation at the land surface. Groundwater recharge may be considered steady where the damping depth is above the depth of the water table. The analytical solution approximates the vadose zone diffusivity as constant, and we evaluated when this approximation is reasonable. We evaluated the analytical solution through comparison of the damping depth computed by the analytic solution with the damping depth simulated by a numerical model that allows variable diffusivity. This comparison showed that the screening method conservatively identifies areas of steady recharge and is more accurate when water content and diffusivity are nearly constant. Nomograms of the damping factor (the ratio of the flux amplitude at any depth to the amplitude at the land surface) and the damping depth were constructed for clay and sand for periodic variations between 1 and 365 d and flux means and amplitudes from nearly 0 to 1×10^{-3} m d^{-1}. We applied the screening tool to Central Valley, California, to identify areas of steady recharge. A MATLAB script was developed to compute the damping factor for any soil and any sinusoidal flux variation.

We present a screening tool for identifying areas in watershed-scale groundwater models where recharge may be simplified as steady state. Nomograms indicate the amount that a variable infiltration is damped with depth for different soils, fluxes, and periods of flux variation. We evaluate the nomograms by comparisons to numerical results from HYDRUS-1D and identify areas of Central Valley, California, where periodic infiltration may become steady recharge.

J.E. Dickinson, U.S. Geological Survey, Arizona Water Science Center, Tucson, AZ 85719; J.E. Dickinson, T.P.A. Ferré, and Becky Crompton, University of Arizona, Dep. of Hydrology and Water Resources, Tucson, AZ 85721; and M. Bakker, Delft Univ. of Technology, Water Resources Section, Faculty of Civil Engineering and Geosciences, 2600 GA Delft, the Netherlands. *Corresponding author (jdickins@usgs.gov).

Vadose Zone J.
doi:10.2136/vzj2013.10.0184
Received 23 Oct. 2013.

Recharge is one of the most poorly defined fluxes in many models of groundwater flow (Lerner et al., 1990; Carrera et al., 2005; Healy, 2010; Ajami et al., 2011). Episodic and periodic variations in fluxes at the land surface result in time-varying water content and transient vertical fluxes within the vadose zone that can result in time-varying recharge. Given the nonlinear relations among flow, hydraulic diffusivity, and water content, fluxes through the vadose zone can be highly uncertain. This uncertainty regarding the location, rate, and temporal variability of recharge can lead to extensive computational effort and introduce uncertainty in transient-flow and solute-transport models.

Uncertainty of time-varying recharge in watershed-scale models reduces the confidence in model predictions such as hydraulic heads, water budget components, solute concentrations, and groundwater ages (e.g., Scanlon, 2000). Computation- or data-intensive efforts for quantifying time-varying recharge are often used to reduce this uncertainty. Current research-level modeling approaches use large-scale, detailed models and extensive computing resources to simulate the interactions of atmospheric, land surface, and groundwater flow processes at fine spatial and temporal scales (e.g., Therrien et al., 2006; Kollet et al., 2010; Maxwell et al., 2011). Time-varying recharge rates may be obtained by using combined watershed and groundwater models with linked surface and subsurface processes such as HydroGeoSphere (Therrien et al., 2006), SWAT/MODFLOW (Sophocleous and Perkins, 2000), MIKE-SHE (Graham and Butts, 2005), GSFLOW (Markstrom et al., 2008), MODFLOW-FMP (Schmid and Hanson, 2009), and ParFlow (Maxwell and Miller, 2005; Kollet and Maxwell, 2006; Ferguson and Maxwell, 2010).

Approaches for simulating recharge and infiltration in regional models include the kinematic wave approximation (Niswonger et al., 2006; Morway et al., 2012) and one-dimensional numerical solution of the Richards equation (Twarakavi et al., 2008; Zhu et al., 2012). Watershed-scale estimates can be obtained from a calibrated transient saturated groundwater-flow model where long-term head and discharge measurements are widely available. However, in the interest of reducing computational efforts, many of these large-scale models greatly simplify unsaturated flow processes, limiting the use of the model for understanding the role of the vadose zone in mediating atmospheric and surface forcings as time-varying recharge to the saturated zone.

Data-intensive methods for quantifying time-varying recharge often require long-term time series data across the temporal range of interest. There has been some investigation of estimating recharge based on long-term time series of groundwater levels (e.g., Dickinson et al., 2004; Knotters and van Walsum, 1997; Crosbie et al., 2005). There has also been extensive use of environmental tracers to estimate recharge fluxes (e.g., Scanlon, 2000; Wahi et al., 2008; Gurdak et al., 2007). The water-level approaches are limited by the scarcity of the necessary long-term data sets in many areas. The tracer approaches provide recharge estimates that are averaged across the time between the introduction and measurement of a tracer at a specific location (Healy, 2010), limiting their use for obtaining watershed-scale recharge distributions for transient models.

In addition to their use in scientific studies, watershed-scale groundwater models are commonly used to assess the transient effects of groundwater development, management practices, and climatic trends on water resources. Because of the complexity of the rates and timing of vertical fluxes through thick vadose zones, groundwater models for resource investigations rarely represent fluxes through the vadose zone directly. Rather, recharge rates are derived from regional water budgets, time averaged across the temporal discretization of the model, and spatially averaged across large subregions of the model (tens to thousands of square kilometers). In some cases, a long-term, steady-state recharge rate is used because time series of groundwater levels are too sparse to infer any realistic temporal variability.

At watershed scales, rapid and episodic variations in fluxes and water content in the vadose zone are commonly approximated to have negligible effects on the heads and water budget (e.g., Pool and Dickinson, 2007). At these scales, the vadose zone is often presumed to smooth out most water content variations from consecutive events of episodic infiltration at the surface. This damping is a justification for assigning slowly varying or constant recharge rates to watershed-scale models. In some cases, the assumption of steady flow may be valid because the variations in fluxes and water content damp with depth in the vadose zone. Bakker and Nieber (2009) presented an analytical solution for such damping that assumes that the water content variations are small enough that hydraulic diffusivity can be approximated as constant. We examined the limits of this approximation for predicting the damping of fluxes with depth and determined how their solution could be used as a practical screening method for identifying where recharge can be approximated as steady state in groundwater models.

Site-specific assessment of the time-varying component of recharge across all anticipated hydroclimatological conditions can be computationally expensive (Kollet et al., 2010). We have developed a new approach, whereby we delineate subregions within the model domain for which recharge can be simplified as steady state. This simplification may reduce the cost of model development and computation time that is typically needed to obtain transient recharge rates from complex hydrologic models. We propose that at watershed and larger scales, infiltration from the land surface to the water table is predominantly vertical and that recharge can be considered to be the sum of a steady, average component and a single periodic, sinusoidal perturbation (Dickinson et al., 2004). Further, for this analysis, we assumed that the single sinusoidal component controls whether recharge can be considered to be steady state: this could be a monthly, seasonal, or annual perturbation. The sinusoidal component of infiltration damps to a degree that is a function of the variable flux, soil type, and depth from the land surface (Bakker and Nieber, 2009). A future study will consider multiple, interfering sinusoidal infiltration perturbations that represent a range of coincident hydroclimatological conditions.

This study used a screening method for identifying areas of steady recharge that is based on the analytical solution of time-varying infiltration presented by Bakker and Nieber (2009). The screening method uses the analytical solution to delineate areas within a watershed where the damping depth is above the water table—recharge in these areas can be adequately represented as steady state while other areas will experience time-varying recharge.

The analytical model from Bakker and Nieber (2009) for periodic flow in the vadose zone is summarized below. Their solution was based on a linearization of the Richards equation by setting the vadose zone diffusivity equal to a constant. We have provided illustrative examples of how the amplitude of sinusoidal fluxes damps with depth in sand and clay for periods of 30 and 90 d. We also created two- and three-dimensional nomograms that show the damping depth as a function of the mean flux, the amplitude and period of sinusoidal forcings, and the soil type. The period lengths range from 1 to 365 d to capture a range of cycles such as artificial irrigation patterns to seasonal and annual cycles in precipitation, runoff, and evapotranspiration. We evaluated whether the constant diffusivity in the analytical solution is reasonable for different perturbations in infiltration across a range of soils. We compared the damping depth from the analytical model with the damping depth from a numerical model that allows variable diffusivity and determined how the soil, mean flux, amplitude of the flux variation, and period of the flux variation control the accuracy

of the analytical predictions of damping. We applied the screening method to the Central Valley of California and mapped the amount of infiltration variability that was preserved at the water table. We also investigated the limitations of the screening tool. The appendix describes a MATLAB program that can be used to generate nomograms for any user-selected soil, mean flux rate, flux period, and water table depth.

Analytical Model

Analytical solutions for periodic groundwater flow conditions, based analogously on the periodic heat flow solutions of Carslaw and Jaeger (1959), have wide application for estimating hydraulic head and flux responses to imposed periodic boundary conditions. These solutions commonly include a term that describes the response in head, water content, or flux as a function of the distance from the boundary. The amplitude of the response damps with distance from the boundary, and the shape of the damping function can be used to either infer aquifer properties or predict some transient behavior. Notable examples are the applications by Jacob (1950) and Ferris (1951) to estimate diffusivity and by Carr and Van Der Kamp (1969) to infer hydraulic conductivity and the specific storage from the responses to tidal fluctuations of a one-dimensional homogeneous aquifer.

Townley (1995) presented a general set of solutions for estimating aquifer responses to any combination of periodic specified head, specified flow, and mixed boundary conditions in a one-dimensional homogeneous confined aquifer. The shape of the response in these solutions for saturated flow is controlled by the aquifer length, saturated diffusivity, and period of the boundary variation (Townley, 1995). Swanson and Bahr (2004) applied Townley's (1995) solutions for periodic areally distributed recharge to explain how seasonal variations in recharge can dampen to a constant discharge rate at distant springs. Hughes et al. (1998) applied a periodic head boundary on one side of a one-dimensional aquifer to estimate the potential dampening of variable heads from tidal forcings into an estuary. Bakker (2004) presented analytical element solutions for periodic flow that can be applied to simulate periodic flow in general settings. Dickinson et al. (2004) applied a periodic specified head boundary condition to represent time-varying water levels and infer the saturated diffusivity and time-varying recharge rates. They demonstrated that water-level variations can be used to infer climatic forcings similar to the El Niño–Southern Oscillation (Cayan et al., 1999) and Pacific Decadal Oscillation (Dettinger et al., 2001; Hanson et al., 2004, 2006) in unconfined alluvial aquifers in the southwestern United States. Bakker (2006) presented a characteristic length beyond which periodic variations in the discharge of a pumping well can be neglected. Bakker and Nieber (2009) derived solutions for vertical periodic and steady flow in the vadose zone and demonstrated how flux, water content, and pressure head variations dampen with depth from a sinusoidal flux boundary at the land surface.

We developed a screening method for identifying regions of groundwater models that can be approximated by steady-state recharge that is based on an analytical solution for periodic vadose flow presented by Bakker and Nieber (2009). The solution is summarized here to review all pertinent approximations and is written into the more common form of a simple wave; a full derivation may be found in Bakker and Nieber (2009).

Consider one-dimensional periodic flow in the vadose zone. The z axis points vertically downward. Flow is governed by the one-dimensional Richards equation, which may be written as

$$\frac{\partial\theta}{\partial\psi}\frac{\partial\psi}{\partial t}=\frac{\partial}{\partial z}\left(K\frac{\partial\psi}{\partial z}\right)-\frac{\partial K}{\partial z} \qquad [1]$$

where θ (dimensionless) is the water content, ψ [L] is the pressure head, $K(\psi)$ [L T^{-1}] is the hydraulic conductivity, and t is time [T]. The vertical flux q_z [L T^{-1}] at the surface is specified to consist of a steady component q_s [L T^{-1}] plus a sinusoidal component with amplitude q_p [L T^{-1}] and period P [T]:

$$q_z(z=0,t)=q_s+q_p\sin(\omega t) \qquad [2]$$

where $\omega = 2\pi/P$ is the angular frequency; the vertical flux at infinite depth is q_s. The steady and periodic components of q can represent the net infiltration below the root zone that results from the infiltration of precipitation, runoff, and the uptake of water by evapotranspiration. Alternatively, time-varying evapotranspiration can be represented as a negative sinusoidal flux with daily or seasonal periods. These components may represent steady and sinusoidally varying infiltration in basin floors, stream channels, and areas of conjunctive water use. The steady component may represent a long-term average flux and the periodic component may represent variations from the steady component. The vertical flux $q(z = \infty,t)$ at infinite depth is defined as the constant steady component q_s. Thus, the water content is constant at infinite depth and the screening tool is meant to represent the vadose zone above the capillary fringe and the water table.

The hydraulic conductivity function is approximated with the Gardner model (Gardner, 1958):

$$K=K_s\exp\left[\alpha(\psi-\psi_e)\right] \qquad \psi<\psi_e \qquad [3]$$

where K_s [L T^{-1}] is the hydraulic conductivity at saturation, ψ_e [L] is the air-entry pressure, and α [L^{-1}] is a fitting parameter based on the pore size distribution. The water content θ is a function of the pressure head and is approximated with the Gardner–Kozeny model (Mathias and Butler, 2006):

$$\theta=n_0\exp\left[\mu(\psi-\psi_e)\right] \qquad \psi<\psi_e \qquad [4]$$

where n_0 is the porosity (dimensionless) and μ is a fitting parameter [L^{-1}].

An analytical solution may be obtained by writing the Richards equation in terms of Kirchoff potentials and through linearization of the resulting differential equation by setting the vadose zone diffusivity D [L^2 T^{-1}] equal to a constant (full details were given in Bakker and Nieber, 2009):

$$D = \frac{K}{C} = \frac{K_s}{n_0 \mu}\left(\frac{\theta_{st}}{n_0}\right)^{\alpha/\mu - 1} \quad [5]$$

where C is the water capacity [L^{-1}] and θ_{st} is the water content corresponding to steady flow q_s:

$$\theta_{st} = n_0\left(\frac{q_s}{K_s}\right)^{\mu/\alpha} \quad [6]$$

The resulting solution is

$$q = q_s + q_p \delta \sin(\omega t - kz) \quad [7]$$

where δ is the damping factor and k is the wave number. The damping factor decreases with depth:

$$\delta = \exp\left(\frac{-z}{\lambda}\right) \quad [8]$$

where λ [L] may be computed as

$$\lambda = \frac{2}{\alpha\left[1+\left(\frac{8\pi}{\alpha^2 DP}\right)^2\right]^{1/4}\cos\left[\frac{1}{2}\arctan\left(\frac{8\pi}{\alpha^2 DP}\right)\right]-\alpha} \quad [9]$$

The damping is controlled by the Gardner (1958) soil parameter α and the nondimensional term $8\pi/\alpha^2 DP$ and is independent of the amplitude of the flux variation q_p. We define the damping depth as the depth z below which <5% of the applied variation is preserved. This means that $\delta = 0.05$, which corresponds to a depth of $d = 3\lambda$ (Fig. 1). However, for any specific application, it would be a simple matter to change this threshold value.

The wave number k [L^{-1}] may be computed as

$$k = \frac{\alpha}{2}\left[1+\left(\frac{8\pi}{\alpha^2 DP}\right)^2\right]^{1/4}\sin\left[\frac{1}{2}\arctan\left(\frac{8\pi}{\alpha^2 DP}\right)\right] \quad [10]$$

The wave speed, v [L T^{-1}], is the velocity at which a wetting or drying front propagates downward. It may be computed as

$$v = \frac{2\pi}{Pk} \quad [11]$$

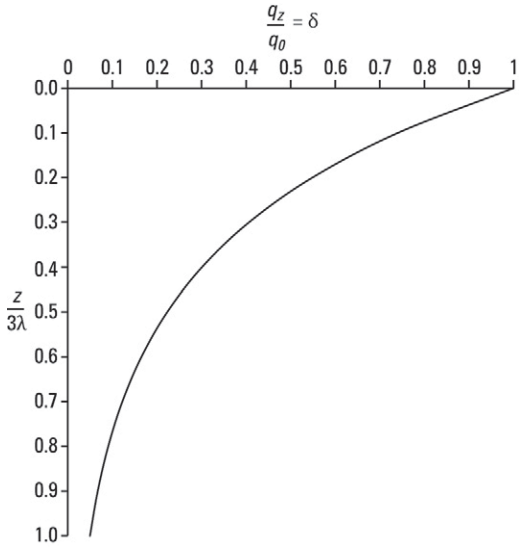

Fig. 1. Plot of the damping factor δ as a function of the ratio between depth and the damping depth $3\lambda = d$. The damping factor is equal to 1 at depth $z/3\lambda = 0$ and decreases exponentially to 0.05 at $z = 3\lambda = d$.

Note that the damping and wave speed in the analytical model are independent of the amplitude of the flux variation q_p.

The term $8\pi/\alpha^2 DP$ in Eq. [9] and [10] is a nondimensional ratio that is analogous to the nondimensional term $L^2/D_s P$ presented by Townley (1995), where L is the length of a one-dimensional aquifer [L] and D_s is the diffusivity of the aquifer under saturated conditions [L^2 T^{-1}]. Townley (1995) demonstrated that $L^2/D_s P$ controls the aquifer response to periodic boundary conditions in a confined aquifer and is related to u in the Theis well function $W(u)$. Large values of $L^2/D_s P$ result in rapid damping of responses near the boundary, while the responses are less damped with distance from the boundary when this ratio is small (Townley, 1995; Dickinson et al., 2004). Similar insights about the persistence of infiltration variations with depth in the vadose zone can be gained from the damping factor (Bakker and Nieber, 2009).

Damping of Sinusoidal Flux Responses with Depth

The manner in which the soil hydraulic properties and the q_p, q_s, and P characteristics of the infiltration flux control the damping is demonstrated below. We show responses for clay and sand soils and a range of periodic vertical fluxes typical of arid and semiarid regions that may result from natural infiltration of precipitation and runoff or from infiltration in areas of conjunctive water use. This region presents challenging conditions for evaluating the screening method because long drying periods between episodic infiltration events can result in highly variable water contents and diffusivities. The appendix describes a code for extending this to different soils, fluxes, and periods in other hydrologic settings. In

the following examples, the steady component of the flux, q_s, is held constant through time, with values ranging from 0.1×10^{-3} m d^{-1} (3.65 cm yr^{-1}) to 1.0×10^{-3} m d^{-1} (36.5 cm yr^{-1}). The amplitude of the sinusoidal component q_p is chosen to be either equal to q_s or equal to 0.1×10^{-3} m d^{-1} (Fig. 2A). The 30-d period might represent an irrigation pattern, and the 90-d periods might represent seasonal cycles in precipitation and runoff. We show these periods to demonstrate how flux variations may damp throughout a depth of 200 m (Fig. 2 and 3). Interannual and interdecadal variations in water levels in arid and semiarid regions (Dickinson et al., 2004; Hanson et al., 2004, 2006) suggest that infiltration, and recharge, is often transient at these longer periods. The magnitudes of q_s and q_p are independent, with the limitation that q_p never exceeds q_s, resulting in a flux that is always either zero or positive in the downward direction. This range of flux rates was chosen to represent the range of recharge rates inferred at focused sites in stream channels and across basin floors in the arid and semiarid southwestern United States (Pool, 2005; Stonestrom et al., 2007; Faunt et al., 2010).

The unsaturated flow properties of the sand and clay soils shown in the nomograms and used in the evaluation of the screening method were defined by the Gardner (1958) and Gardner–Kozeny (Mathias and Butler, 2006) soil models (Table 1). Values of K_s were taken from the Rosetta soil catalog (Schaap et al., 2001). The Gardner α and Gardner–Kozeny n_0 and μ parameter values were estimated by a linear regression with the van Genuchten α and assuming a constant value of van Genuchten $n_0 = 4$ for each soil based on the soil properties reported by Bakker and Nieber (2009). For site-specific applications, Gardner and Gardner–Kozeny soil properties can be estimated using ROSETTA or the fitting procedure of Wraith and Or (1998).

In all cases, the flux amplitudes are largest at the land surface and damp with depth (Fig. 2 and 3) as described by Eq. [8], while the mean flux rate q_s remains constant with depth. The flux variations damp more in clay than sand across the same depth interval. For example, the flux variations in clay when $P = 30$ d, $q_s = 0.5 \times 10^{-3}$ m d^{-1}, and $q_p = 0.5 \times 10^{-3}$ m d^{-1} damp to 5% of the applied flux variation at depth $z = 1.04$ m; in sand, the flux amplitude damps to 5% at depth $z = 6.42$ m (Fig. 2B and 2C).

The analytical solution results in a symmetrical pattern of maximum and minimum values around the mean flux (Fig. 2). For example, for a flux variation with period of 30 d in the sand, four peaks in the flux pattern can be identified within the 10-m depth at time $3P/4$, indicating that the prior four pulses of infiltration at the surface were preserved. In the clay, only one maximum peak in the flux was preserved at time $3P/4$. For further discussions, we will represent the damping of the flux peaks with depth using an envelope that connects the maximum (and minimum) flux at each depth through all times (Fig. 2).

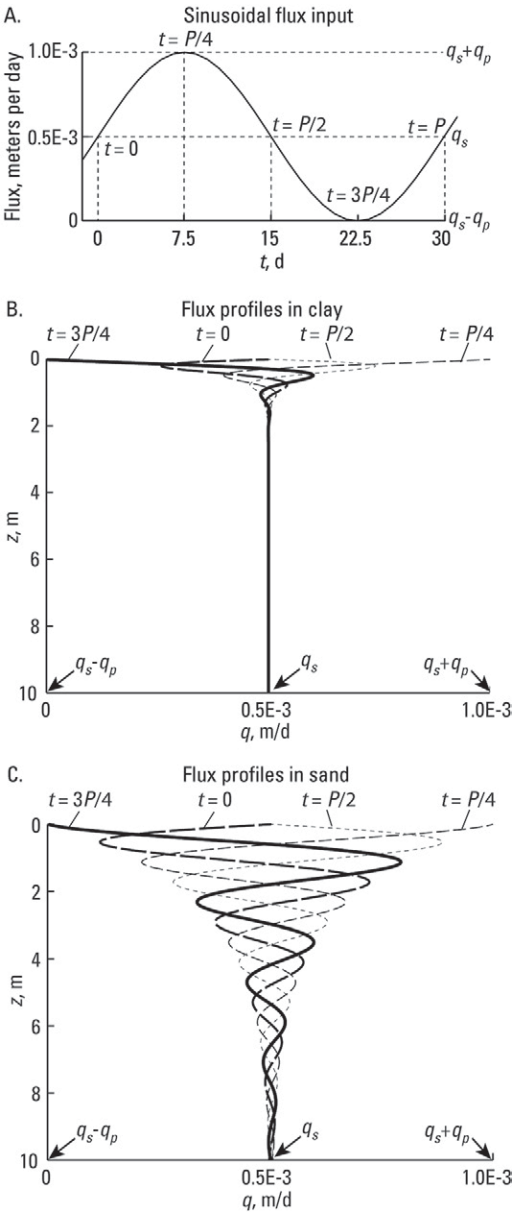

Fig. 2. Damping of a sinusoidal flux (A) applied at the land surface ($z = 0$), (B) in clay and (C) in sand. Profiles of the flux with depth at four different times (0, $P/4$, P, and $3P/4$, where P is the sinusoidal period) show how the flux varies with depth at different times t. The flux has a steady component q_s plus a sinusoidal component with amplitude q_p.

The damping of the periodic fluxes with depth is controlled by the soil type, period, and the mean flux (Eq. [9]). In the examples shown in Fig. 3, q_p and q_s are 0.5×10^{-3} or 1.0×10^{-3} m d^{-1} and the period of the variation is 30 or 90 d, resulting in four different periodic flux patterns at the land surface in which the flux varies between 0 m d^{-1} and $2q_s$. The flux envelope resulting from a 30-d period is shaded dark gray and the envelope from the 90-d period is shaded light gray (Fig. 3A). The damping depth d and the area contained by the envelope are larger when the flux boundary varies with the longer (90-d) period than the shorter (30-d) period. The damping depth and area of the envelope increase when the mean flux q_s increases from 0.5×10^{-3} to 1.0×10^{-3} m d^{-1}.

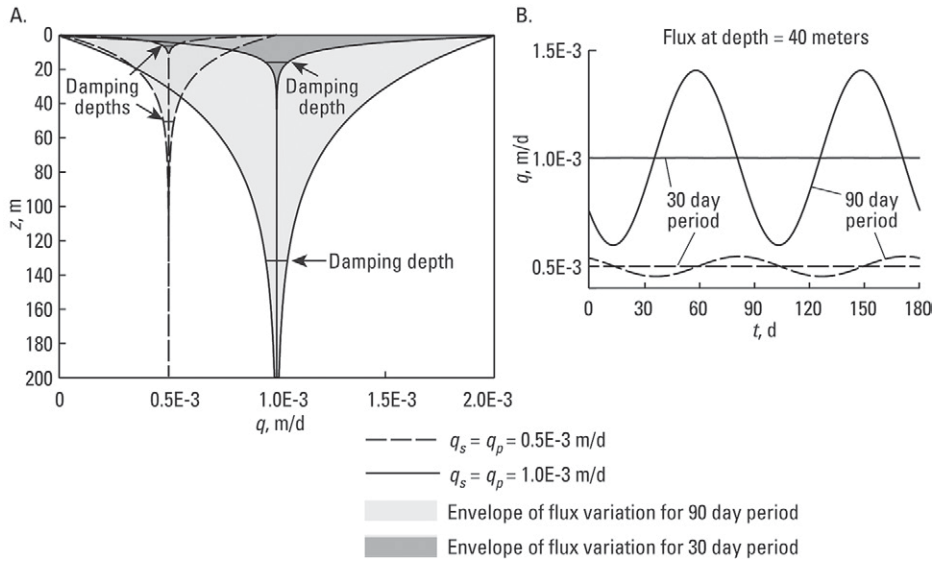

Fig. 3. (A) Plot of the envelope that surrounds the range of flux variations with depth in a sand soil and the damping depth from four different configurations of the flux boundary, and (B) the resulting flux time series at a depth of 40 m. The diffusivity is constant in each of the four cases. The flux has a steady component q_s plus a sinusoidal component with amplitude q_p.

For groundwater modeling, we are ultimately concerned with the flux across the water table. Therefore, it is useful to consider how the amplitudes of the flux time series differ at a common depth for different flux boundary configurations (Fig. 3B). Taking a depth of 40 m as an example, the amplitude variation is largest when the mean flux is higher and the period of variation is longest. At this depth, the amplitude variation is effectively zero for both mean fluxes when the flux varies at 30-d periods. That is, recharge could be considered to be steady state despite the temporal variations in infiltration.

Damping Factor and Damping Depth Nomograms

Nomograms of the damping factor δ and damping depth d are presented as a simple screening tool to identify the conditions for which recharge can be approximated as steady or must be treated as transient. The damping factor nomogram (Fig. 4) can be used to estimate the damping of the amplitude of a periodic flux between depths of 0 m and 10 m in sand or clay. The damping depth nomogram (Fig. 5) provides the depth at which a periodic flux is damped to 5% of its amplitude at the land surface. These nomograms indicate the damping due to a single periodic flux cycle where $q_p = q_s$ in a vertically homogenous clay or sand.

The damping factor nomogram (Fig. 4) indicates how the damping factor decreases with depth z, but it also shows how the damping factor at the same depth increases as the mean flux and period of the flux variation increases. For example, at a depth of 2 m in clay, the damping factor for the same 365-d period increases from approximately 0.4 when the mean flux equals 2×10^{-4} m d^{-1} to nearly 0.9 for a mean flux of 1×10^{-3} m d^{-1}. That is, more of the flux variation is preserved at the same depth at a higher mean flux. At a depth of 6 m in sand, the damping factor at a mean flux of 6×10^{-4} m d^{-1} increases from 0.1 for a 30-d period, to 0.7 to 0.8 for a 90-d period, and to 0.9 to 1.0 for a 365-d period. In other words, more of the flux variation is preserved at a single depth as the period increases.

The damping depth nomogram (Fig. 5) indicates that the damping depth increases for longer periods and larger mean fluxes. The nomogram shows the $\log_{10}$ of the damping depth as the mean flux increases from nearly 0 to 1×10^{-3} m d^{-1} and the period increases from nearly 0 to 365 d. The damping depth in clay increases to >10 m for periods >300 d and mean fluxes >6×10^{-4} m d^{-1}. In sand, for the same range of flux periods and means, the damping depth increases to >1000 m and recharge should be considered as transient for all practical purposes.

Table 1. Gardner (G) (Gardner, 1958) and van Genuchten (vG) (van Genuchten, 1980) parameters for clay and sand in the examples.

Soil	vG α	K_s	vG $\theta_s = n_0$	G α	G μ	ψ_e
	m^{-1}	m d^{-1}		——m^{-1}——		m
Clay	1.50	0.15	0.459	6.87	2.05	−0.37
Sand	3.52	6.43	0.375	14.39	4.28	−0.12

Evaluation of the Screening Method

The screening method for identifying steady recharge was evaluated for clay and sand soils and a range of periodic vertical fluxes typical of arid and semiarid regions. The variable fluxes are representative of monthly, seasonal, or annual variations that may be observed in frequently collected time series data or in longer term monitoring. The damping depths and flux variations were evaluated for sand and clay through comparison with the results of numerical simulations using HYDRUS-1D (Šimůnek et al., 2005).

The numerically derived damping depth d_{num} is the depth in the numerical model where the ratio of the flux variation at any depth z to the flux variation at $z = 0$ is reasonably equal to 0.05. The numerical solution was assumed to be the more accurate solution because HYDRUS-1D computes a variable diffusivity based on a nonlinear relation between diffusivity and

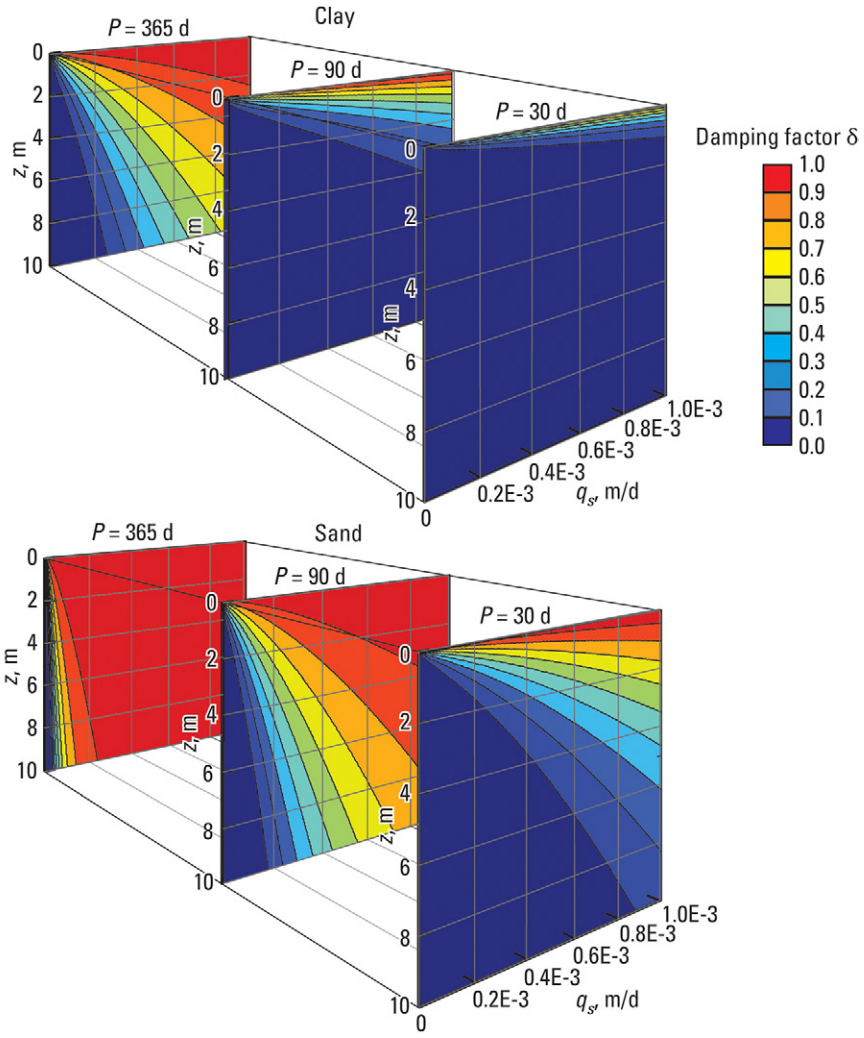

Fig. 4. Damping factor nomogram for estimating the damping at depths from 0 to 10 m in a homogenous sand or clay soil. The damping factor is the fraction of the flux variation at depth z and the surface flux variation at $z = 0$. Areas in blue indicate that almost all of the surface flux variation is damped, red indicates that most of the variation is preserved, while green, yellow, and orange indicate that some of the variation is preserved. The top panel shows the damping for clay and the bottom shows damping for sand. Each two-dimensional plot shows the damping at depth for a mean flux q_s from 0 to 1×10^{-3} m d^{-1} for periods P of 30, 90, and 365 d.

water content rather than assuming a constant diffusivity. The Gardner and Gardner–Kozeny models were used to define the pressure head–hydraulic conductivity and pressure head–water content relations, respectively, for sand and clay soils simulated by the numerical model. A specified flux was defined at the top boundary and free drainage was defined as the bottom boundary condition. For this analysis, the damping depth from the analytical model was defined to be acceptable when it overpredicted the damping depth by no more than a factor of two. The factor of two was chosen because it provides a conservative estimate without excessively overestimating the damping depth. If the damping depth is overestimated, it also underestimates the damping factor. That is, an overestimate of the damping depth would result in identifying some areas as requiring the consideration of transient recharge that could actually be treated as steady state. For example, if the analytical model suggests that the entire domain can be treated as steady state, then this assumption can be made with confidence, despite the simplifications adopted in the analytical model.

Comparison of Responses with Depth

The flux, water content, diffusivity, and wave speed profiles from the analytical and numerical models were compared at times $3P/4$ and $P/4$ in sand (Fig. 6). The soil and fluxes shown in Fig. 6 are identical to those shown in Fig. 2C. In Fig. 6, the pattern and damping of the flux variability begins to differ between the analytical and numerical models with increasing depth.

The profiles include symmetrical and asymmetrical patterns around the steady values below approximately 6 m. In the analytical model, the vertical flux profiles (Fig. 6A) are symmetrical around the mean value, whereas the water content (Fig. 6B) is asymmetrical and the diffusivity (Fig. 6C) and wave speed (Fig. 6D) are constant. In contrast, the vertical profiles of flux, water content, diffusivity, and wave speed from the numerical model are all asymmetrical around the steady values. For example, in the numerical model, the first flux minimum was below the surface at $z = 0.85$ m, while the first flux maximum occurred at $z = 1.3$ m, while in the analytical model they both occurred at $z = 1.1$ m.

The numerical model produced a smaller envelope surrounding the range of flux and water content variations (Fig. 6A and 6B). The water content was skewed toward lower water contents near the land surface. As a result, the water content decreased more during low flux than it increased during high flux at any given depth. This skew toward lower water contents resulted in a lower time-averaged diffusivity than the diffusivity associated with the mean flux, which is used in the analytical model. The lower time-averaged diffusivity in the numerical model increases the damping and reduces the damping depth. Thus, a higher time-averaged diffusivity in the analytical model results in deeper propagation of flux variations, and the analytical model is conservative because it overpredicts the damping depth. For the purposes of using the analytical model as a screening tool, it is important to note that, for the reasons detailed above, the numerical model will always result in a lower damping depth—in this example, $d/d_{num} = 6.42$ m/4.82 m = 1.33 (Fig. 6A).

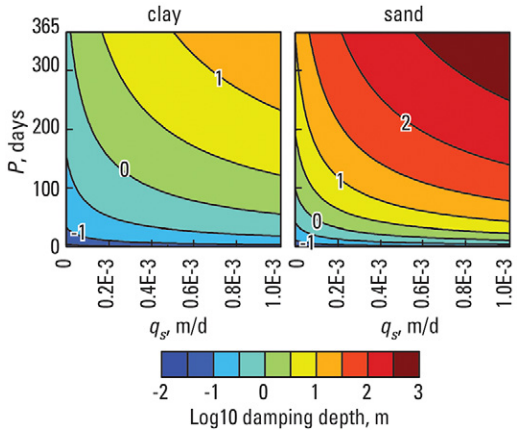

Fig. 5. Damping depth nomogram for estimating the damping depth in a homogenous sand or clay soil, which is the depth at which a periodic flux boundary at the land surface is damped to 5% of its original amplitude. Areas in blue indicate that the damping depth is relatively shallow (<1 m), red indicates that the damping depth is deep (up to 1000 m), while green, yellow, and orange indicate that the damping depth is generally between 1 and 10 m.

In the analytical model, the diffusivity was too high during dry conditions and too low during wet conditions. In the numerical model, the water content minimum below the surface near $z = 1$ m corresponded to a diffusivity (3.23×10^{-3} m^2 d^{-1}) that was lower than the diffusivity in the analytical model (5.20×10^{-3} m^2 d^{-1}). The lower diffusivity had the effect of reducing the wave speed of this flux minimum, as indicated by Eq. [10] and [11]—this slowing can be observed in the profile at time $P/4$ as the flux minimum near $z = 1$ m in the numerical model traveled a shorter vertical distance from the surface than the corresponding minimum in the analytical model during the same amount of time. A higher water content, near $z = 1.25$ m in the profile at time $3P/4$, resulted in a higher diffusivity (6.75×10^{-3} m^2 d^{-1}) than the diffusivity in the analytical model (5.20×10^{-3} m^2 d^{-1}) at the same depth. This increase in diffusivity also increased the wave speed of this flux maximum, and the flux maximum from the numerical model traveled a greater vertical distance than the flux maximum from the analytical model during the same time.

The differences in damping produced by the analytical and numerical models can be further explained through the physical processes that result in damping and how these processes are represented in the models. The key assumption of the analytical solution is that the diffusivity, the ratio of K to the water capacity, is constant. The analytical and numerical models use the Gardner model for K as a function of ψ (Gardner, 1958). Therefore, K varies in both time and space in both models as ψ varies. The effect of approximating a constant diffusivity with a variable K is to introduce systematic errors in the water capacity, which can be inferred by Eq. [5]. Under dry conditions, the water capacity is underestimated to balance the decrease in K. As the system wets, the water capacity is overestimated to offset the increase in K. In the numerical model, the water capacity is equal to $d\theta/d\psi$ from the Gardner–Kozeny model (Mathias and Butler, 2006). These differences in how the water capacity is represented in the analytical and numerical models lead to differences in the damping factor and damping depth.

Comparison of Damping Depths

To compare the analytical and numerical damping depths, the flux components were defined two ways: (i) q_p and q_s are equal and range from 0.1×10^{-3} to 1.0×10^{-3} m d^{-1}, or (ii) q_p is held constant at 0.1×10^{-3} m d^{-1} and q_s ranges from 0.1×10^{-3} to 1.0×10^{-3} m d^{-1}. These flux conditions were used to investigate how sensitive the analytical solution estimation error is to the amplitude of the flux variability and to find the conditions where the screening tool can be considered to be both conservative and acceptably accurate. We expressed the relative error of the screening method using a ratio of d/d_{num}, which is the factor by which the analytical model overestimates the damping depth—a ratio of 2 indicates that the analytical model overestimated by a factor of 2. Higher values indicate greater overestimation of the damping depth and underestimation of the damping by the analytical solution. The ratio d/d_{num} was closest to 1 in clay when the flux boundary variations had a small periodic component q_p, a small steady component q_s, and the shortest periods (blue areas in Fig. 7). The analytical damping depth was least accurate (d/d_{num} >5) in sand when q_p, q_p, and the period P were large (red areas in Fig. 7). In both clay and sand, the accuracy decreased as q_p, q_s, and P increased. In clay, d was within a factor of 2 for all flux configurations, suggesting that the analytical solution adequately predicted the damping depth in clay for these fluxes. In sand, however, d was >2 when $q_p = 0.1 \times 10^{-3}$ m d^{-1} and $q_s > 0.8 \times 10^{-3}$ m d^{-1}, and for most of the flux rates when the period was >100 d. These results indicate that the screening tool is more conservative (greater overestimation of the damping depth and underestimation of the damping factor) for both larger periods and larger mean fluxes. The screening tool will more accurately predict the depth at which low fluxes with short periods of variation are damped. Thus, the screening tool can be used with the most confidence to examine whether small, rapidly varying infiltration that may result from low, frequent precipitation or irrigation variations results in transient recharge.

Soil and Flux Controls on Damping Accuracy

The manner in which the soil and flux components q_p, q_s, and P control the accuracy of the damping depth from the analytical model were explored by identifying how these properties control the diffusivity and its variability (Fig. 8). Because the analytical model uses a single value of diffusivity, it is more representative of real soil and flux configurations in which the variation of the diffusivity is relatively small. In the numerical model, and in real systems, variable fluxes produce variations in the water content, which, in turn, change the diffusivity. Consequently, the damping depth from the analytical model was expected to be more accurate in systems where the diffusivity is less variable.

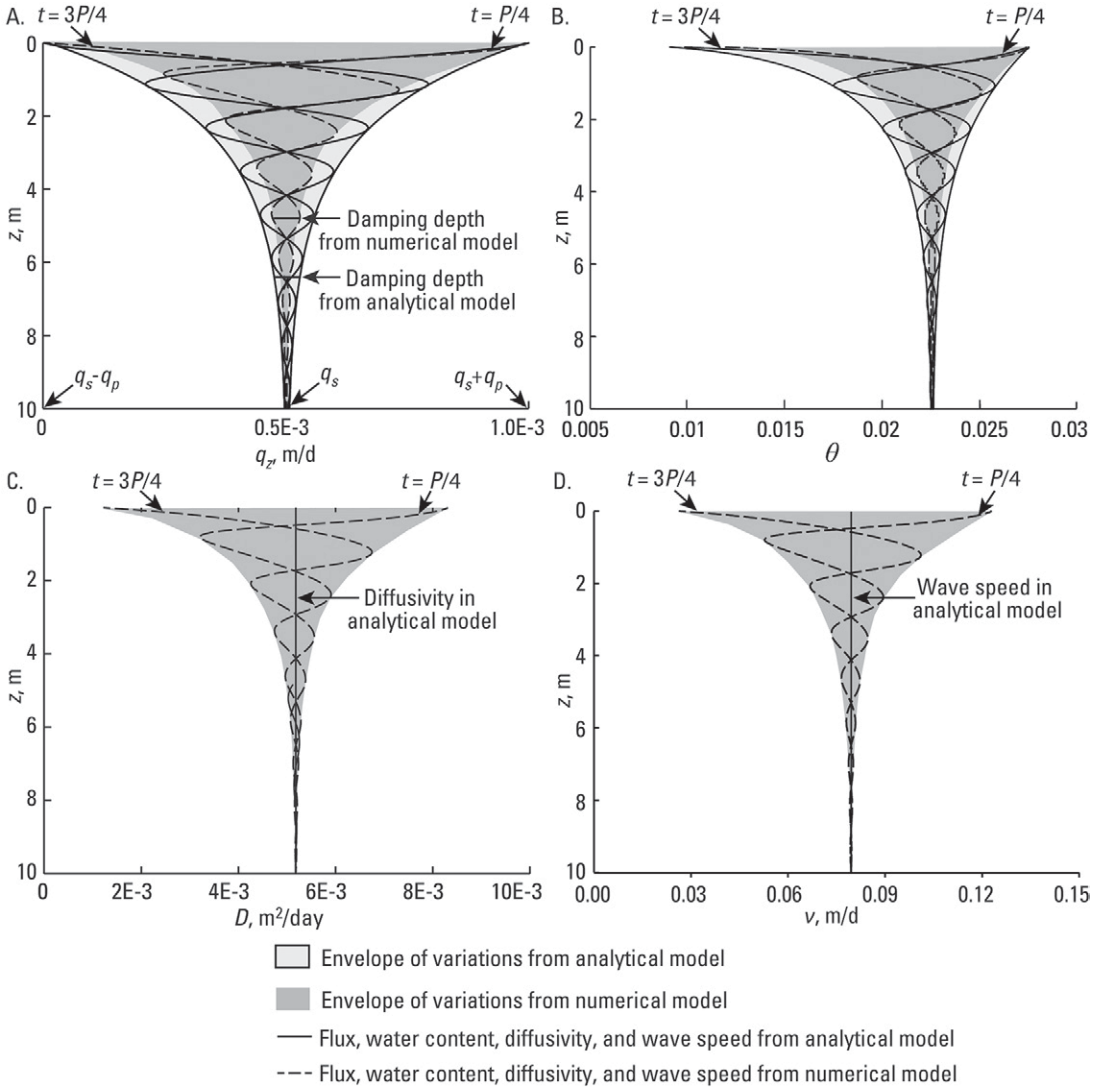

Fig. 6. Comparison of (A) flux q_z, (B) water content θ, (C) diffusivity D, and (D) wave speed v profiles at times $P/4$ and $3P/4$, where P is the sinusoidal wave period, and the envelopes encompassing the variations in the profiles produced by the analytical model and the numerical model HYDRUS-1D. The outputs are for a sand soil, a period of 30 d, and mean flux of 0.5×10^{-3} m d^{-1}. The numerical model simulated a more shallow damping depth and more narrow range of flux and water content variations than the analytical model. All profiles from the numerical model and the water content from the analytical model are asymmetrical around the mean value at depths >6 m. The diffusivity and wave speed were constant in the analytical model, which resulted in symmetrical flux variations around the mean flux.

Variations in diffusivity owing to changes in the water content can be estimated by the nonlinear relation between water content and diffusivity (Fig. 8), as indicated by Eq. [5]. In the Gardner–Kozeny soil model, diffusivity increases monotonically and exponentially as the water content increases. Furthermore, both relative and absolute changes in the water content under drier conditions result in smaller variations in diffusivity than the same changes in water content at higher water contents. The amount of variation in diffusivity, given a change in water content, differs between clay and sand—the diffusivity varies more in sand than clay for a given change in water content.

The relation between water content and diffusivity provides insight into why the analytical solution is more accurate at lower mean flux q_s and flux variation q_p. For clay and sand soils in which the mean flux $q_s = 0.5 \times 10^{-3}$ m d^{-1} and the flux variation was either $q_p = q_s$ (Fig. 8, light gray areas) or $q_p = 0.1 \times 10^{-3}$ m d^{-1} (Fig. 8, dark gray areas), the water content was always <0.1. In sand when $q_s = q_s = 0.5 \times 10^{-3}$ m d^{-1}, the water content varied between 0.012 and 0.026 and diffusivity varied from 1.21×10^{-3} to 8.29×10^{-3} m^2 d^{-1}. As the flux variation q_p decreased to 0.1×10^{-3} m d^{-1}, the water content variation (0.021–0.023) and diffusivity variation (4.48×10^{-3}–5.83×10^{-3} m^2 d^{-1}) both decreased. In clay, for these same values of q_s and q_p, the water content was higher and varied more than in sand, but the diffusivity varied less. In clay when $q_p = q_s$ the water content varied from 0.067 and 0.097 and the diffusivity varied between 1.70×10^{-3} and 3.97×10^{-3} m^2 d^{-1}. As q_p decreased to 0.1×10^{-3} m d^{-1},

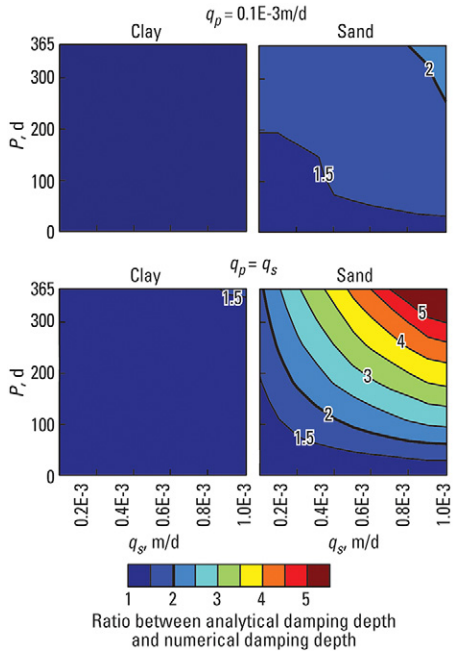

Fig. 7. Error of the damping depth computed by the analytical model, expressed as the ratio of the analytical damping depth to the "true" numerical damping depth for clay and sand soils. Values near 1 indicate that the damping depths are similar, and values near 5 indicate that the analytical damping depth is overestimated by nearly a factor of five times. The heavy black line along the ratio of 2 indicates the limit above which we consider the damping depth to be acceptable. In the top panels, the amplitude of the flux boundary q_p in the numerical model was held constant at 0.1×10^{-3} m d^{-1}. In the bottom panels, the amplitude of the flux boundary q_p at the surface is equal to the mean flux q_s. The error is less in all configurations when the period P of the flux variation is shorter and increases with longer periods. The error is less in both clay and sand when q_p is less than q_s, which occurs for nearly all cases in the top panels. The error increases as q_p and q_s become larger.

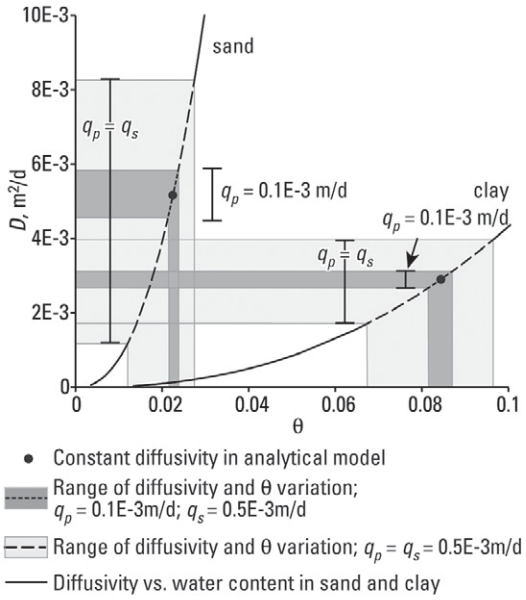

Fig. 8. Ranges of water content θ and diffusivity D variations from the numerical model (shown as dashed and dotted lines in shaded areas) showing that a constant diffusivity in the analytical model (solid dot) is more representative of the diffusivity in the numerical model when the diffusivity variation and flux amplitude q_p are lower. Diffusivity is shown as a function of water content for sand and clay. The diffusivity variations in the numerical model result from a variable flux boundary of period 30 d. The constant value of diffusivity in the analytical model is based on the water content that is associated with the mean flux q_s. The amplitude of the flux variation q_p is either equal to 0.1×10^{-3} m d^{-1} or equal to the mean flux $q_s = 0.5 \times 10^{-3}$ m d^{-1}. In both soils, the diffusivity varied less when $q_p = 0.1 \times 10^{-3}$ m d^{-1} than when $q_p = q_s = 0.5 \times 10^{-3}$. The range of diffusivity, for the same flux boundary, was less in clay than in the sand. The diffusivity variation for which $q_p = q_s$ in sand is identical to the diffusivity variation shown in Fig. 6 at $z = 0$.

both the water content variations (0.082–0.087) and diffusivity variations (2.67×10^{-3}–3.11×10^{-3} m^2 d^{-1}) decreased (Fig. 8). These relations suggest that for the same mean flux and variation, the analytical solution will be more accurate in clay than sand. More generally, the analytical solution will be more accurate across a range of fluxes that give rise to a smaller change in diffusivity with time. This includes most areas of fine soils, which typically have fairly constant water contents, or areas of coarser soils in relatively wet regions where water contents also tend to be more constant with time.

Within the limitations of the analytical solution discussed above, we have developed a screening tool that can be applied to regional-scale models. The tool takes as input the steady-state and expected primary periodic recharge, soil type, and water table depth at each location. The output is the damping factor at the depth of the water table for each cell. Based on this output, the user can identify areas of constant recharge. Further consideration of soil type, steady flux, and flux variation amplitude can be used to refine estimates of damping for those areas that are identified as receiving transient recharge.

Identifying Areas of Steady Recharge

The screening tool for identifying areas of steady recharge was applied to the Central Valley in California. This example demonstrates how areas of steady recharge can be identified if the available data are limited to maps of soil type and depth to groundwater and estimates of the period and mean value of infiltration. This simple screening approach does not require the extensive data necessary for complex models of the interactions of atmospheric, land surface, and groundwater flow processes. This example is not intended to represent the variations of infiltration and recharge that result naturally or from conjunctive use in the groundwater flow model of the Central Valley by Faunt (2009) and Hanson et al. (2012) but to demonstrate the use of the screening tool for a well-characterized system. Because the analytical model is conservative in defining areas of constant recharge, the screening tool can be applied with some confidence to eliminate subregions within a model for consideration of time-varying recharge. Data- and computation-intensive modeling approaches can then be limited to the remaining areas in the domain.

The damping factor maps were created by calculating the damping factor from the analytical model for each 1.6- by 1.6-km cell for which the appropriate data were available. The extent of the spatial grid and colored area of the maps coincide with the soil texture map of Faunt et al. (2010) and the domain of simulated groundwater flow in the three-dimensional groundwater flow model of Faunt (2009). Depths to the water table were obtained from a grid of simulated water table depths during the year 1961 by the groundwater flow model (Faunt, 2009). In study areas that do not have these grids available, continuous maps of soil type and contour maps of water table depths can be interpolated and used similarly.

The surface flux boundary had mean q_s and variation q_p both equal to 1.0×10^{-3} m d^{-1} and periods of 30, 90, and 365 d. The 30-d period might represent an irrigation pattern, and the 90- and 365-d periods might represent seasonal and annual cycles in precipitation and runoff. While the long-term average recharge rates vary spatially in the Central Valley (Faunt, 2009), this example used the same flux boundary in each cell to demonstrate how areas of steady or transient recharge can change for different periods. In a real application of the screening tool, spatially variable estimates of the mean infiltration could be used. Differences in the distribution of steady recharge in the model of Faunt (2009) and the distribution predicted by the screening tool were probably due to different fluxes in the model and the manner in which the flux controls the damping (Fig. 4) and damping depth (Fig. 5).

Three maps of the damping factor in the Central Valley (Fig. 9) indicate the amount of a surface flux variation that was preserved at the depth of the water table for the three investigated periods. On

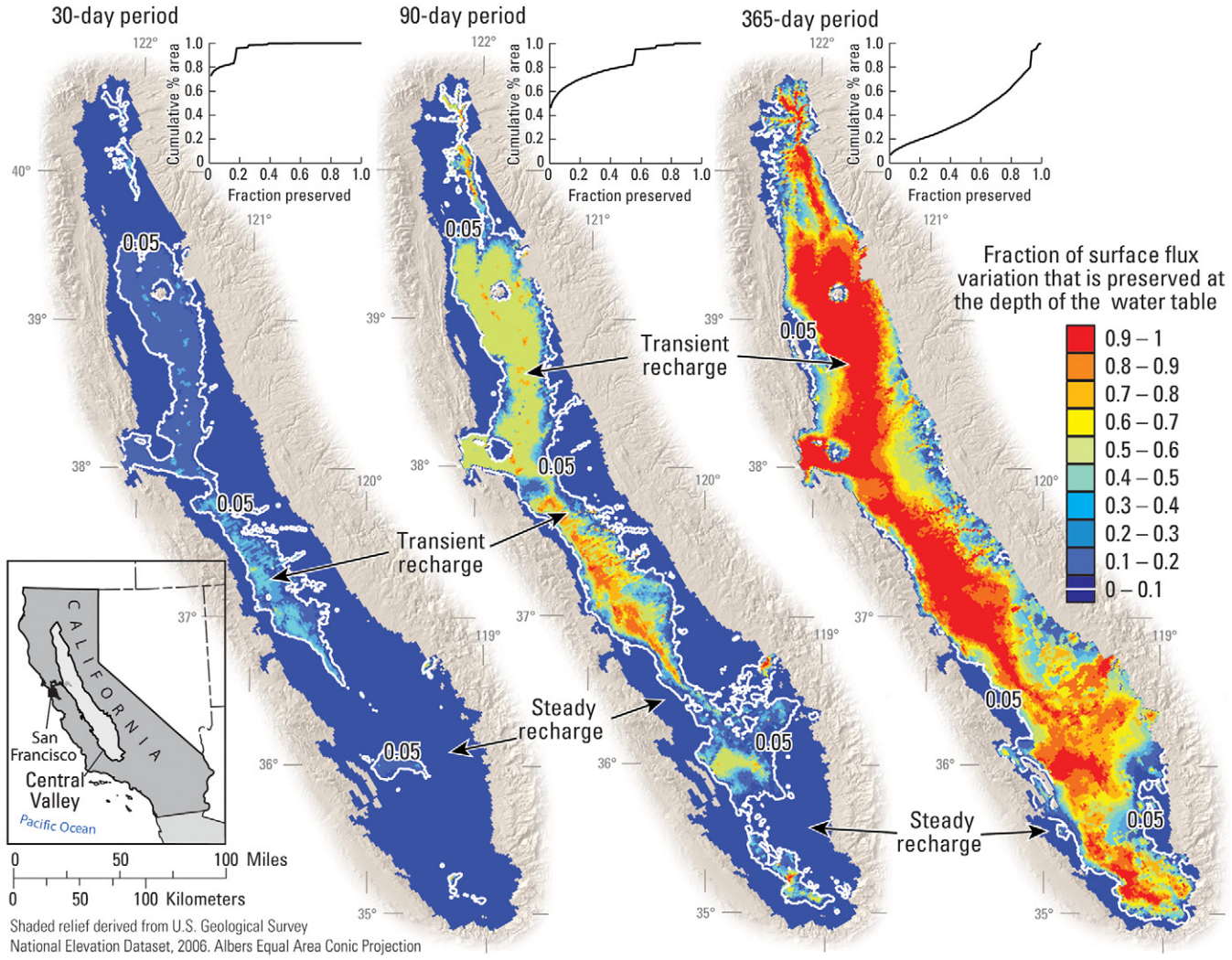

Fig. 9. Maps of the damping factor at the water table in Central Valley, California, computed by the analytical model. The damping factor is the fraction of the surface flux variation that is preserved at any depth. The white lines indicate where the damping factor is equal to 0.05 and separate areas where recharge is either steady or transient. The periods of the flux variation are 30 d (left), 90 d (middle), and 365 d (right), and the mean flux q_s and flux variation q_p are both equal to 0.5×10^{-3} m d^{-1} in all cases. Blue areas indicate that nearly all of the flux variation is damped at the water table and that recharge is steady. Red areas indicate that most of the variation is preserved at the water table and that recharge is transient. Green, yellow, and orange areas indicate that some of the variation is preserved and recharge is transient, but the amplitude of the recharge variations is damped. The flux amplitudes are more damped (blue areas) for the shorter 30-d period and along the basin margins where the water table is deep. The flux amplitudes are preserved (red areas) as the period becomes longer and within the center of the basin where the water table is shallower.

the maps, areas in blue indicate that the damping factor was low and that most of the surface flux variation was damped in the vadose zone—this means that recharge could be considered to be steady at the depth of the water table. Areas in red show where the damping factor was high, meaning that a small amount of the surface flux variation was damped in the vadose zone and the recharge should be considered to be transient. Intermediate amounts of damping are indicated by areas in orange, yellow, and green.

The damping factor was smaller along the margins of the aquifer where the unsaturated zone is thick and the water table depths are deepest—up to 150 m in the southern part of the Central Valley (Faunt, 2009). Large damping factors along the northwest axis coincide with shallow water tables (Faunt, 2009), where flux variations are barely damped by the thin unsaturated zone. The damping factor from the 30-d period was <0.1 in most of the domain, indicating that most variations damped in the unsaturated zone and that recharge at this period damped out (blue areas) in most of the Central Valley. As the period increased to 90 d, the damping factor increased to up to 0.8 along the northwest axis through the center of the Central Valley, indicating that variations at this period resulted in transient recharge. The damping factor for the 365-d period was between 0.9 and 1.0 along most of the northwest axis, indicating that nearly all of the variations at the surface were preserved at the depth of the water table and recharge was transient. Despite the deep water table in the southern part of the valley, the damping factor for the 365-d period was >0.5 (more variation was preserved) in several isolated areas because of coarser soils that preserved more infiltration variation.

The damping factor for the Central Valley is likely to be accurate in areas of finer soils and for shorter periods when q_s and q_p are both equal to 1.0×10^{-3} m d^{-1}. The soils in the Central Valley grade texturally between clay and sand and are generally finer in the northern half of the domain (Faunt et al., 2010). The evaluation of the damping depth accuracy for these two soils provides insight into whether the mapped damping fractions in the Central Valley are within our threshold for accuracy. Figure 7 indicates that at our values of q_s and q_p, the damping depth is accurate for the 30-d period for both clay and sand. For periods of 90 and 365 d, the damping depths are accurate for clay. In sand, d/d_{num} for the 90-d period is slightly greater than the limit of 2, and >5 for the 365-d period, which means that the analytical solution was underestimating the amount of damping for these periods. Thus, some areas indicated by green or orange could be treated as having steady-state recharge. The damping factor for all three periods is likely to be accurate in many parts of the northern half of the Central Valley because of its finer textured soils. In the southern half, the damping factor for the 30- and 90-d periods may be accurate, but the results for the 365-d period may benefit from additional screening using a numerical solution.

The screening tool indicates that for the shorter infiltration periods, and the fluxes in this example, recharge can be simplified as steady across much of the Central Valley. The 30- and 90-d periods became steady across approximately 80 and 60% of the model, respectively. Both shorter periods are likely to result in transient recharge in the center of the system where conjunctive water use is important for groundwater simulations (Hanson et al., 2012). This conservative estimate of the area indicates that recharge from short infiltration periods may be averaged through time and simplified as a mean recharge rate in these areas of a groundwater model. This simplification may allow the use of longer model time steps or fewer interactions of atmospheric, land-surface, and groundwater-flow processes in the model. The 365-d period became steady in approximately 10% of the model area, indicating that while some modeling resources can be saved, complex modeling methods may be necessary to characterize the transient recharge from this longer component. However, a groundwater model is likely to require less computational effort to represent this slowly varying recharge component than more rapid fluctuations.

The screening tool may also indicate where fewer data are needed to develop and calibrate a groundwater model. Efforts for inferring infiltration components that vary at 30-d periods may involve hydrometeorological measurements at daily and weekly intervals to characterize its variability. Infiltration components that vary at 90-d intervals may be inferred from measurements at longer monthly intervals. Both of these infiltration components were damped along the basin margin, which suggests that data collection, as well as modeling of land–atmosphere interactions, along the basin margin at daily, weekly, and monthly intervals, may not be useful for inferring time-varying recharge. However, recharge from the 30-, 90-, and 365-d infiltration components were transient along the central axis of the system, suggesting that data intensive, and perhaps computationally intensive, approaches to inferring recharge may be necessary to characterize time-varying recharge at these periods. The map of the damping factor for the 365-d period indicates that infiltration variations at this longer period result in transient recharge across much of the Central Valley. The preservation of longer periods across most of the domain indicates that data collection or data-intensive modeling efforts at monthly intervals may be necessary to characterize time-varying recharge cycles at the 365-d and longer interannual to interdecadal periods related to climate variability (e.g., Hanson et al., 2004, 2006; Dickinson et al., 2004).

Conclusions

We developed a screening tool for identifying areas of steady recharge within watershed-scale models. The screening tool is based on the analytical solution by Bakker and Nieber (2009), which describes the time-varying flux through a homogeneous unsaturated zone in response to sinusoidal infiltration. Variations in flux and water content damp with depth, leading to effectively steady fluxes below some depth. The damping factor is the ratio between the amplitude of the flux variation at a specific depth

and the amplitude of the flux variation at the land surface. The damping factor is equal to 1 at the land surface and decreases exponentially with depth. The damping depth is defined here as the depth at which the damping ratio is equal to 0.05, below which we consider the flux to be effectively steady. We consider recharge to be approximately steady if the water table is below this damping depth. The damping factor at any depth, as well as the damping depth, increases as the mean and the period of the sinusoidal infiltration increase. Both the damping factor and depth are larger in sand than in clay when the same period and mean flux are applied.

The analytical solution of Bakker and Nieber (2009) is based on a constant hydraulic diffusivity with time. We evaluated the limits of this approximation by comparing the damping depth from the analytical model to that of a numerical model that allows diffusivity to vary with time. The damping depths were compared in clay and sand examples where the mean flux q_s and variation q_p ranged from 0.1×10^{-3} to 1×10^{-3} m d^{-1} and the period of the variation ranged from 1 to 365 d. As expected, the damping depth obtained from the analytical model was most accurate when the diffusivity in the numerical model was least variable. The diffusivity variability decreased when the mean, amplitude, and period of the sinusoidal surface flux boundary were reduced. The analytical solution overpredicted the damping depth in all cases, making it a conservative indicator of regions experiencing steady recharge. We consider the analytical solution to be an acceptable estimator of the damping depth if it overestimates the damping depth by less than a factor of 2. Using this criterion, the analytical solution was acceptable in clay for all cases and acceptable in sand for nearly all cases when q_p was small (0.1×10^{-3} m d^{-1}) and $q_p = 1 \times 10^{-3}$ m d^{-1}.

Nomograms of the damping factor and the damping depth were presented as a screening tool for identifying if the sinusoidal flux variation effectively damped to zero at the depth of the water table. The damping factor nomogram (Fig. 4) identified the amount of damping between the depths of 0 and 10 m. The damping depth nomogram (Fig. 5) provided the depth at which a flux variation damped below 5%. In the damping factor nomogram, the flux varied at 30-, 90-, and 365-d periods and the mean ranged from 0 to 1×10^{-3} m d^{-1}. In the damping depth nomogram, the period of the flux variations ranged from 1 to 365 d and the mean ranged from 0 to 1×10^{-3} m d^{-1}. The damping for a real system can be estimated by identifying the damping factor for a period and mean flux within these ranges. If the damping factor at the depth of the water table is <0.05, or if the damping depth is above the depth of the water table, then recharge is effectively steady.

An application of the screening tool to the Central Valley, California, was used to demonstrate how to apply the tool for a well-characterized system with extensive soil texture and water table data. Such an application can be used to identify where a groundwater model can be simplified, potentially leading to more efficient computation time and data collection. The screening tool identified areas of steady recharge, where periodic infiltration at the land surface was effectively damped to zero at the depth of the water table. The infiltration varied at periods of 30, 90, and 365 d, and maps of the damping factor for each period indicated the amount of damping of the flux variation at the depth of the water table (Fig. 9). Most of the variation for the 30-d period was damped throughout the domain, suggesting that the recharge from this infiltration pattern is generally steady. The maps of the damping factor from the 90- and 365-d periods indicated that recharge is mostly transient in areas of shallow water tables and coarse soils and steady where the water table is deep along the margins. The extent of the areas where recharge was interpreted to be steady is probably smaller than the areas that may be determined by a numerical model with coupled surface and subsurface processes (Faunt, 2009). Consequently, recharge from the three periodic infiltration components might be steady across a larger portion of the domain. The results from the screening tool suggest that data are not needed to characterize the shorter periods but may be necessary to quantity the longer periods of infiltration variations. For example, observations of short-term changes in soil moisture may not be necessary in many areas because the recharge may vary at longer time frames.

The screening tool indicates where a groundwater model can be simplified by treating recharge as steady. This can reduce the computation effort and may indicate that fewer data are needed to characterize recharge in some areas. Hydrometeorological measurements at short intervals may not be needed to characterize infiltration variations that damp to a steady flux at the water table. Groundwater models may be simulated using longer time steps if rapid flux changes are damped in areas of the model of interest. For assessments of time-varying recharge, the complex interactions between atmospheric, land-surface, and groundwater-flow processes may not be necessary if their effects on fluxes in the vadose zone, and on recharge, are sufficiently damped. These simplifications can reduce the time and cost of data collection, model development, and computation time. Further investigations will examine the influence of multiple interacting time-varying infiltration patterns and the impacts of layered heterogeneities on the screening accuracy.

Appendix

The MATLAB computer program DAMP creates two-dimensional nomograms of the damping factor by using the analytical model of Bakker and Nieber (2009). The nomograms indicate the amount of damping at a single depth or within a range of depths in any user-specified soil and configuration of the period and mean of the sinusoidal flux boundary. The purpose of this program is to create nomograms for any combination of these inputs that can be applied to real systems to identify areas where recharge is steady. This appendix provides a brief overview of how to use the program.

DAMP is executed by running the MATLAB .m file named DAMP.m within the MATLAB environment. DAMP requires the MATLAB software, which is available at www.matlab.com. The program was written and tested using Version R2012a, and it may run on previous and future versions of MATLAB. No compilation or installation of DAMP is necessary. The script can be downloaded at http://az.water.usgs.gov/software/damp.html.

User Interface

The user interface contains menus of options for computing the nomograms. The main menu is displayed on executing the program. The main menu contains the following list of options:

1. Select and Define Soils
2. Define Infiltration Period
3. Define Infiltration Flux
4. Define Water Table Depth
5. Calculate and Display Results

Other. Exit Program

Select and Define Soils

Selecting Option 1 will display a table that shows a list of soil types and parameters that are preloaded in the program. The soils are preloaded from an external ASCII file named SoilsTable.txt containing tab-delimited soil names and parameter values. The units of the parameters of the default list of soils are meters and days. A list of options for modifying the soil list is displayed below the soil table. The list can be modified within the program by using the menu to add or remove soils, rename the soils, and change the values of the soil parameters of any preloaded or new soil. The soil list can also be edited directly in the ASCII file before executing the program.

Nomograms are generated only for the soils listed in the table that are active. Soils are activated and deactivated by selecting Option 1: Activate/Deactivate Soils, which displays a list of the active and inactive soils. Soils are activated and deactivated by entering the number of the soil in the list.

Define Infiltration Period

Selecting Option 2 will prompt the minimum and maximum periods that define the range of periods included on the nomograms. Default values of 1 d for the minimum and 10 d for the maximum will be assigned if blank values are entered. The nomogram will compute the damping depth at 11 periods at equal increments defined by the minimum and maximum periods.

Define Infiltration Flux

Selecting Option 3 will prompt the minimum and maximum mean infiltration values that define the range of infiltration means included on the nomograms. Default values of 0.1×10^{-3} m d^{-1} for the minimum and 1×10^{-3} m d^{-1} for the maximum will be assigned if blank values are entered. The nomogram will compute the damping depth at 11 mean flux values at equal increments defined by the minimum and maximum mean fluxes.

Define Water Table Depth

Selecting Option 4 will prompt the minimum and maximum depth values that define the range of depths included on the nomograms. Default values of 1 m for the minimum and 10 m for the maximum will be assigned if blank values are entered. The nomogram will compute the damping depth at 11 depths at equal increments defined by the minimum and maximum mean fluxes.

Calculate and Display Results

Selecting Option 4 will prompt the value (period, flux, and depth) of the axes in the nomograms. The damping factor nomogram (Fig. 4) can be replicated by selecting the flux for the x axis and the depth for the y axis. The value that is not displayed on an axis is fixed to the midpoint of its range. For example, if period is not displayed, the midpoint value is 183 d for the default with minimum and maximum values of 1 and 365 d, respectively.

The nomograms are displayed as color-filled plots of the damping factor for a specific soil and are automatically saved as.jpg files in the working directory that contains the DAMP.m file. A nomogram is displayed for each active soil. The nomograms can be displayed with different values along the axes by entering 1; the nomograms will not be recalculated if this option is selected, which saves computation time.

Acknowledgements

We thank reviewers Richard G. Niswonger and Randall T. Hanson of the USGS and an anonymous reviewer. This work was funded by the Southwest Climate Science Center.

References

Ajami, H., P.A. Troch, T. Maddock III, T. Meixner, and C. Eastoe. 2011. Quantifying mountain block recharge by means of catchment-scale storage–discharge relationships. Water Resour. Res. 47(4):W04504. doi:10.1029/2010WR009598

Bakker, M. 2004. Transient analytic elements for periodic Dupuit–Forchheimer flow. Adv. Water Resour. 27:3–12. doi:10.1016/j.advwatres.2003.10.001

Bakker, M. 2006. Where do periodic variations in the discharge of a well become negligible? Ground Water 44:478–482. doi:10.1111/j.1745-6584.2005.00159.x

Bakker, M., and J.L. Nieber. 2009. Damping of sinusoidal surface flux fluctuation with soil depth. Vadose Zone J. 8:119–126. doi:10.2136/vzj2008.0084

Carr, P.A., and G.S. Van Der Kamp. 1969. Determining aquifer characteristics by the tidal method. Water Resour. Res. 5:1023–1031. doi:10.1029/WR005i005p01023

Carrera, J., A. Alcolea, A. Medina, J. Hidalgo, and L.J. Slooten. 2005. Inverse problem in hydrogeology. Hydrogeol. J. 13:206–222. doi:10.1007/s10040-004-0404-7

Carslaw, H.S., and J.C. Jaeger. 1959. Conduction of heat in solids. 2nd ed. Oxford Univ. Press, New York.

Cayan, D.R., K.T. Redmond, and L.G. Riddle. 1999. ENSO and hydrologic extremes in the western United States. J. Clim. 12:2881–2893. doi:10.1175/1520-0442(1999)012<2881:EAHEIT>2.0.CO;2

Crosbie, R.S., P. Binning, and J.D. Kalma. 2005. A time series approach to inferring groundwater recharge using the water table fluctuation method. Water Resour. Res. 41(1):W01008. doi:10.1029/2004WR003077

Dettinger, M.D., D.S. Battisti, R.D. Garraud, G.J. McCabe, and C.M. Bitz. 2001. Interhemispheric effects of interannual and decadal ENSO-like climate variations on the Americas. In: V. Markgraf, editor, Interhemispheric climate linkages. Academic Press, San Diego. p. 1–16.

Dickinson, J.E., R.T. Hanson, T.P.A. Ferré, and S.A. Leake. 2004. Inferring time-varying recharge from inverse analysis of long-term water levels. Water Resour. Res. 40(7):W07403. doi:10.1029/2003WR002650

Faunt, C.C., editor. 2009. Groundwater availability of the Central Valley Aquifer, California. Prof. Pap. 1766. USGS, Reston, VA.

Faunt, C.C., K. Belitz, and R.T. Hanson. 2010. Development of a three-dimensional model of sedimentary texture in valley-fill deposits of Central Valley, California, USA. Hydrogeol. J. 18:625–649. doi:10.1007/s10040-009-0539-7

Ferguson, I.M., and R.M. Maxwell. 2010. Role of groundwater in watershed response and land surface feedbacks under climate change. Water Resour. Res. 46(10):W00F02. doi:10.1029/2009WR008616

Ferris, J.G. 1951. Cyclical fluctuations of water level as a basis for determining aquifer transmissibility. IAHS Publ. 33:148–155.

Gardner, W.R. 1958. Some steady-state solutions of the unsaturated moisture flow equation with application to evaporation from a water table. Soil Sci. 85:228–232. doi:10.1097/00010694-195804000-00006

Graham, D.N., and M.B. Butts. 2005. Flexible, integrated watershed modelling with MIKE SHE. In: V.P Singh and D.K. Frevert, editors, Watershed models. CRC Press, Boca Raton, FL. p. 245–272.

Gurdak, J.J., R.T. Hanson, P.B. McMahon, B.W. Bruce, J.E. McCray, G.D. Thyne, and R.C. Reedy. 2007. Climate variability controls on unsaturated water and chemical movement, High Plains Aquifer, USA. Vadose Zone J. 6:533–547. doi:10.2136/vzj2006.0087

Hanson, R.T., M.D. Dettinger, and M.W. Newhouse. 2006. Relations between climatic variability and hydrologic time series from four alluvial basins across the southwestern United States. Hydrogeol. J. 14:1122–1146. doi:10.1007/s10040-006-0067-7

Hanson, R.T., L.E. Flint, A.L. Flint, M.D. Dettinger, C.C. Faunt, D.R. Cayan, and W. Schmid. 2012. A method for physically based model analysis of conjunctive use in response to potential climate changes. Water Resour. Res. 48(6):W00L08. doi:10.1029/2011WR010774

Hanson, R.T., M.W. Newhouse, and M.D. Dettinger. 2004. A methodology to assess relations between climatic variability and variations in hydrologic time series in the southwestern United States. J. Hydrol. 287:252–269. doi:10.1016/j.jhydrol.2003.10.006

Healy, R.W. 2010. Estimating groundwater recharge. Cambridge Univ. Press, New York.

Hughes, C.E., P. Binning, and G.R. Willgoose. 1998. Characterisation of the hydrology of an estuarine wetland. J. Hydrol. 211:34–49. doi:10.1016/S0022-1694(98)00194-2

Jacob, C.E. 1950. Flow of ground water. In: H. Rouse, editor, Engineering hydraulics. John Wiley & Sons, Hoboken, NJ. p. 321–386.

Knotters, M., and P.E.V. van Walsum. 1997. Estimating fluctuation quantities from time series of water-table depths using models with a stochastic component. J. Hydrol. 197:25–46. doi:10.1016/S0022-1694(96)03278-7

Kollet, S.J., and R.M. Maxwell. 2006. Integrated surface–groundwater flow modeling: A free-surface overland flow boundary condition in a parallel groundwater flow model. Adv. Water Resour. 29:945–958. doi:10.1016/j.advwatres.2005.08.006

Kollet, S.J., R.M. Maxwell, C.S. Woodward, S. Smith, J. Vanderborght, H. Vereecken, and C. Simmer. 2010. Proof of concept of regional scale hydrologic simulations at hydrologic resolution utilizing massively parallel computer resources. Water Resour. Res. 46(4):W04201. doi:10.1029/2009WR008730

Lerner, D.N., A.S. Issar, and I. Simmers. 1990. Groundwater recharge: A guide to understanding and estimating natural recharge. Int. Assoc. of Hydrogeol., Hannover, Germany.

Markstrom, S.L., R.G. Niswonger, R.S. Regan, D.E. Prudic, and P.M. Barlow. 2008. GSFLOW, Coupled ground-water and surface-water flow model based on the integration of the Precipitation–Runoff Modeling System (PRMS) and the Modular Ground-Water Flow Model (MODFLOW-2005). Tech. Meth. 6-D-1. USGS, Reston, VA.

Mathias, S.A., and A.P. Butler. 2006. Linearized Richards' equation approach to pumping test analysis in compressible aquifers. Water Resour. Res. 42(6):W06408. doi:10.1029/2005WR004680

Maxwell, R.M., J.K. Lundquist, J.D. Mirocha, S.G. Smith, C.S. Woodward, and A.F. Tompson. 2011. Development of a coupled groundwater–atmosphere model. Mon. Weather Rev. 139:96–116. doi:10.1175/2010MWR3392.1

Maxwell, R.M., and N.L. Miller. 2005. Development of a coupled land surface and groundwater model. J. Hydrometeorol. 6:233–247. doi:10.1175/JHM422.1

Morway, E.D., R.G. Niswonger, C.D. Langevin, R.T. Bailey, and R.W. Healy. 2012. Modeling variably saturated subsurface solute transport with MODFLOW-UZF and MT3DMS. Ground Water 51:237–251. doi:10.1111/j.1745-6584.2012.00971.x

Niswonger, R.G., D.E. Prudic, and R.S. Regan. 2006. Documentation of the Unsaturated-Zone Flow (UZF1) package for modeling unsaturated flow between the land surface and the water table with MODFLOW-2005. Tech. Meth. 6A19. USGS, Reston, VA.

Pool, D.R. 2005. Variations in climate and ephemeral channel recharge in southeastern Arizona, United States. Water Resour. Res. 41(11):W11403. doi:10.1029/2004WR003255

Pool, D.R., and J.E. Dickinson. 2007. Ground-water flow model of the Sierra Vista subwatershed and Sonoran portions of the Upper San Pedro basin, southeastern Arizona, United States, and northern Sonora, Mexico. Sci. Invest. Rep. 2006-5228. USGS, Reston, VA.

Scanlon, B.R. 2000. Uncertainties in estimating water fluxes and residence times using environmental tracers in an arid unsaturated zone. Water Resour. Res. 36:395–409. doi:10.1029/1999WR900240

Schaap, M.G., F.J. Leij, and M.Th. van Genuchten. 2001. ROSETTA: A computer program for estimating soil hydraulic parameters with hierarchical pedotransfer functions. J. Hydrol. 251:163–176. doi:10.1016/S0022-1694(01)00466-8

Schmid, W., and R.T. Hanson. 2009. The Farm Process Version 2 (FMP2) for MODFLOW-2005: Modifications and upgrades to FMP1. Tech. Meth. 6A32. USGS, Reston, VA.

Šimůnek, J., M.Th. van Genuchten, and M. Sejna. 2005. The HYDRUS-1D software package for simulating the one-dimensional movement of water, heat, and multiple solutes in variably-saturated media. Dep. of Environ. Sci., Univ. of California, Riverside.

Sophocleous, M., and S.P. Perkins. 2000. Methodology and application of combined watershed and ground-water models in Kansas. J. Hydrol. 236:185–201. doi:10.1016/S0022-1694(00)00293-6

Stonestrom, D.A., J. Constantz, T.P.A. Ferré, and S.A. Leake, editors. 2007. Ground-water recharge in the arid and semiarid southwestern United States. Prof. Pap. 1703. USGS, Reston, VA.

Swanson, S.K., and J.M. Bahr. 2004. Analytical and numerical models to explain steady rates of spring flow. Ground Water 42:747–759. doi:10.1111/j.1745-6584.2004.tb02728.x

Therrien, R., R.G. McLarren, E.A. Sudicky, and S.M. Panday. 2006. HydroGeoSphere: A three-dimensional numerical model describing fully-integrated subsurface and surface flow and solute transport. Groundwater Simulations Group, Waterloo, ON, Canada.

Townley, L.R. 1995. The response of aquifers to periodic forcing. Adv. Water Resour. 18:125–146. doi:10.1016/0309-1708(95)00008-7

Twarakavi, N.K.C., J. Šimůnek, and S. Seo. 2008. Evaluating interactions between groundwater and vadose zone using the HYDRUS-based flow package for MODFLOW. Vadose Zone J. 7:757–768. doi:10.2136/vzj2007.0082

van Genuchten, M.Th. 1980. A closed-form equation for predicting the hydraulic conductivity of unsaturated soils. Soil Sci. Soc. Am. J. 44:892–898.

Wahi, A.K., J.F. Hogan, B. Ekwurzel, M.N. Baillie, and C.J. Eastoe. 2008. Geochemical quantification of semiarid mountain recharge. Ground Water 46:414–425. doi:10.1111/j.1745-6584.2007.00413.x

Wraith, J.M., and D. Or. 1998. Nonlinear parameter estimation using spreadsheet software. J. Nat. Resour. Life Sci. Educ. 27:13–19.

Zhu, Y., L. Shi, L. Lin, J. Yang, and M. Ye. 2012. A fully coupled numerical modeling for regional unsaturated–saturated water flow. J. Hydrol. 475:188–203. doi:10.1016/j.jhydrol.2012.09.048